Bulk heating of solid-density plasmas during high-intensity-laser plasma interactions

P. M. Nilson,* W. Theobald, J. F. Myatt, C. Stoeckl, M. Storm, J. D. Zuegel, R. Betti,*,†
D. D. Meyerhofer,*,† and T. C. Sangster
Laboratory for Laser Energetics, University of Rochester, Rochester, New York 14623, USA
(Received 4 October 2007; revised manuscript received 15 October 2008; published 13 January 2009)

K-shell x-ray spectroscopy is used to study the interaction of small-mass copper foil targets ($>20\times20\times2$ μm^3) with a high-intensity ($>10^{19}$ W/cm^2) laser pulse. Efficient bulk heating to greater than 200 eV is demonstrated using collisional-energy transfer from recirculating fast electrons. *K*-photon yields and bulk-electron temperatures calculated by three-dimensional numerical target-heating simulations are in good agreement with the experimental measurements.

DOI: 10.1103/PhysRevE.79.016406 PACS number(s): 52.50.Jm, 52.38.Kd, 52.57.Kk, 52.70.La

I. INTRODUCTION

Progress in high-power laser technology is rapidly advancing the fundamental understanding of intense radiation-matter interactions. Understanding the coupling efficiency between high-intensity laser pulses and electrons in initially cold, solid-density plasma is of considerable interest and underpins a host of basic high-energy-density (HED) phenomena [1–9]. When a high-intensity laser pulse ($>10^{18}$ W/cm^2) interacts with a solid-density target, a significant fraction of the laser energy is coupled to initially cold electrons. These electrons are accelerated to relativistic energies and find widespread applications, from laboratory astrophysics [10] to high fluence line and continuum radiation generation [11–14], and fast-ignition inertial fusion [15,16]. Techniques to efficiently generate and probe such extreme states of matter are widely pursued.

Previously, much attention was given to studying high currents in solid-density targets with thicknesses a significant fraction of the collisional fast-electron range (i.e., several hundreds of micrometers). Current densities beyond 10^{10}–10^{12} A/cm^2 are readily achievable, far exceeding the Alfvén limit I_A [kA]$=17\beta\gamma$, where $\gamma=(1-\beta^2)^{-1/2}$ is the relativistic factor and $\beta=v/c$ is the electron velocity normalized to the speed of light [17]. Heating by Ohmic dissipation of the collisional return current [18] dominates in this regime, and isochoric heating (i.e., at constant volume) to hundreds of electronvolts has been demonstrated [2–8,19–21].

Recent research has shown that reducing the target foil area and thickness to tens of micrometers increases the importance of Debye sheath fields [9,22,23]. For sufficiently high target potentials, a large number of fast electrons may recirculate inside the plasma while supplying their own return current. This creates a plasma regime, where resistive return-current heating plays only a transient role and collisional slowing-down dominates. Much of the physics of how these plasmas form remains unclear. An improved understanding of their radiative properties, for example, could lead to the development of compact, university-scale HED plasma sources using multiterawatt laser drivers.

Previous studies have characterized the fast-electron-induced heating of small-mass targets using 85- to 400-J, 0.4- to 10-ps pulses, achieving maximum spatially and temporally integrated bulk-electron temperatures of up to 200 eV at solid density [24,25]. Such bulk temperatures were diagnosed using spectral measurements of the fast-electron-induced inner-shell emission using *K*-photon spectroscopy [22,23,26,27]. The observed line broadening and wavelength shifts indicate a significant $K\alpha$ emission from multiply ionized ions, deexciting within regions of plasma with high thermal electron temperatures. More recently, heating of charge-insulated, mass-limited copper targets of 0.12 mm^2 $\times 20$ μm to tens of electronvolts using high-contrast, 400-fs, 13-J laser pulses and $I=5\times10^{17}$ W/cm^2 has been demonstrated [28]. Each of these measurements is consistent with the smallest-volume targets, reaching the highest bulk-electron temperatures.

Modeling indicates [23] that even smaller-mass targets could be bulk heated to hundreds of electronvolts using joule-class, multiterawatt laser systems. The underlying heating mechanism is not fully understood, and the experimental connection with detailed theoretical energy-coupling models, which describe how the fast electrons transfer their energy to the target bulk, has not been obtained.

We report in this paper bulk heating measurements of solid-density material using a high-intensity ($>10^{19}$ W/cm^2, 1 ps) multiterawatt laser pulse in the regime where collisional fast-electron slowing-down dominates. This is achieved using thin, small-area copper foil targets. Efficient bulk heating of dense plasma to hundreds of electronvolts is demonstrated by the strong modification of the cold $K\beta/K\alpha$ ratio as a function of increasing energy density.

The physical process underlying this target-heating mechanism has been studied extensively using three-dimensional, implicit-hybrid particle-in-cell (PIC) simulations and collisional-radiative code modeling. On the basis of the code results and a *K*-photon production model, a minimum laser-energy deposition of $15\pm7\%$ into fast electrons is required to account for the experimentally observed *K*-photon yields when heating is small. Comparison of the $K\beta/K\alpha$ ratio reduction for decreasing target volume and increasing energy density with large-scale numerical target-

*Also at Fusion Science Center for Extreme States of Matter and Fast Ignition Physics, University of Rochester, Rochester, NY 14623, USA.

†Also at Mechanical Engineering and Physics Department, University of Rochester, Rochester, NY 14623, USA.

heating calculations indicates a fast-electron energy content of $20 \pm 10\%$ over a wide range of target volumes. Maximum bulk-electron temperatures exceeding 200 eV are inferred using 5-J, 1-ps pulses and $(20 \times 20 \times 2)$-μm^3 copper targets. Agreement between these two results provides confidence in the scaling of the laser-to-electron-energy-conversion efficiency in the refluxing regime, and thus the total energy that is available for bulk heating—a quantity of direct interest for future multikilojoule-class experiments.

II. EXPERIMENTAL DETAILS

The experiment was performed at the Laboratory for Laser Energetics using the Multi-Terawatt (MTW) Laser Facility [29]. The laser delivered 1- to 5-J, 1-ps pulses at a wavelength of 1.054 μm and was focused using an $f/2$ off-axis parabola at normal incidence to the target. The laser-pulse duration was monitored on a shot-to-shot basis using a single-shot autocorrelator. The focal-spot full width at half-maximum was between 4 and 6 μm, giving a peak intensity of 2×10^{19} W/cm^2. The targets were copper foils that ranged between $20 \times 20 \times 2$ and $1000 \times 1000 \times 20$ μm^3 and were mounted using either a 17-μm-diam silicon carbide stalk or, in the case of the smallest targets, a pair of 1-μm-diam spider silk threads.

Prepulses at subrelativistic intensities alter a solid-density target prior to the onset of the main interaction pulse. To understand the preplasma constraints of the MTW laser system, high-dynamic-range optical parametric chirped-pulse-amplification (OPCPA) contrast measurements have been reported [30]. The compressed OPCPA pulse temporal profile has been measured, using a third-harmonic cross-correlator, to consist of three components: a Fourier-transform-limited pulse at time t_0 with a contrast of around 10^{-3} and a pedestal divided into two regions. In the pedestal, the pulse intensity decreases by 10 dB per 15 ps to $(t_0 - 25)$ ps, and 10 dB per 25 ps to $(t_0 - 100)$ ps, reaching an approximately constant value of 10^{-8}. This contrast level is maintained to the maximum temporal range of the contrast diagnostic at $(t_0 - 170)$ ps. This 100-ps-level pedestal is likely caused by temporal noise on the OPCPA pump pulse preventing optimum recompression on the picosecond time scale. This contrast level causes the main laser pulse to interact with a short-scale-length plasma rather than an extended-scale-length preformed plasma that may be created by a longer time duration prepulse.

Previous two-dimensional radiation-hydrodynamics simulations [25] show that at intensities of 10^{13} W/cm^2, a 500-ps duration laser prepulse can penetrate initially solid-density targets to micrometer-scale depths (see, for example, Ref. [25] and references therein). While no on-shot diagnostics were fielded to monitor preplasma formation in this experiment, focused intensities of 10^{13} W/cm^2 are achieved around 40 ps prior to the main MTW pulse. This prepulse level severely constrains the total mass of material that may be preablated and the total target penetration depth that may be reached on this time scale.

The K-shell line radiation generated during the interaction was diagnosed with a single-photon-counting spectrometer

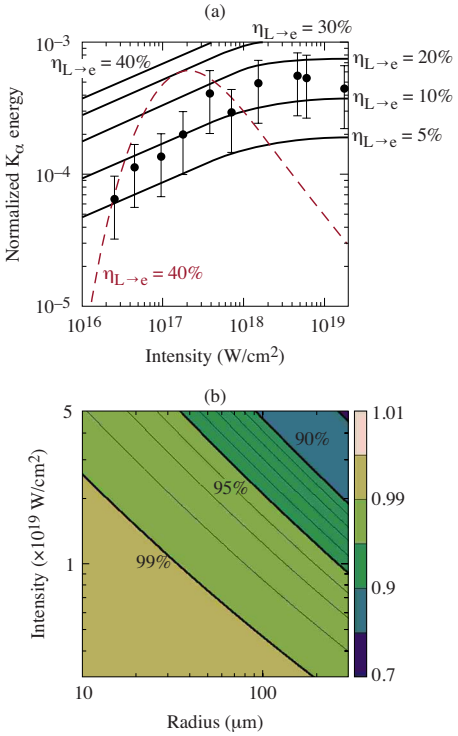

FIG. 1. (Color online) (a) Energy in $K\alpha$ photons as a function of laser intensity using $(500 \times 500 \times 20)$-$\mu m^3$ copper targets irradiated by 1-J, 1-ps pulses. Calculated K-photon yields (solid lines) as a function of laser intensity, assuming electron refluxing and various laser-to-electron-energy-conversion efficiencies $\eta_{L\to e}$. Calculated K-photon yield as a function of laser intensity for $\eta_{L\to e}$=40% in the absence of refluxing (dashed curve). (b) Calculated refluxing efficiency as a function of laser intensity and target foil area using the simple capacitance model presented in Ref. [23].

[31] based on an SI 800-145 x-ray back-illuminated, charge-coupled device (CCD). Quantum efficiency measurements for this camera using single-pixel analysis at 8 keV, and absolute calibration measurements using radioactive Fe^{55} (5.9 keV Mn $K\alpha$) and Cd^{109} (22.1 keV Ag $K\alpha$) sources, have been previously reported [22,32].

The spectrometer was located 80 and 240 cm from the laser-solid interaction at an angle of either 23° or 43° to the target normal. Extensive shielding optimized the signal-to-noise ratio and suppressed the hard-x-ray background. Various copper filters of between 75 and 150 μm optimized the detected signal-to-background ratio of the K-shell emission, depending on the target volume under study. In calculating the absolute number of emitted $K\alpha$ and $K\beta$ photons, the emission is assumed to be isotropic. Corrections due to target opacity effects, the filter-transmission function, the CCD quantum efficiency, and the solid angle that was sampled by the detector were made, with the statistical measurement error given by Poisson statistics.

III. RESULTS

Figure 1(a) shows the measured total energy in $K\alpha$ photons that are emitted by a $(500 \times 500 \times 20)$-$\mu m^3$ copper tar-

get (normalized to the laser energy and corrected for the filter transmission) as a function of the laser intensity. The $K\alpha$ yield steadily increases for intensities above 10^{16} W/cm^2 and becomes intensity-independent above 10^{18} W/cm^2.

The experimental data in Fig. 1(a) are compared to a model of $K\alpha$ production [22,23]. The model accounts for refluxing by allowing the fast electrons to slow down in energy inside the target, transferring energy through collisions. The model makes no assumption about the spatial homogeneity of the energy deposition. An exponentially distributed fast-electron spectrum is assumed, $f(E)=(1/T_e)\exp(E/T_e)$, where $T_e=\langle E\rangle$ is correlated with the laser irradiance through either the ponderomotive scaling

$$T_e(\mathrm{MeV}) = 0.511[(1 + I_{18}\lambda_{\mu m}^2/1.37)^{1/2} - 1] (I > 10^{18}\ \mathrm{W/cm^2})\ \text{(Ref. [26])}$$

or the phenomenological scaling T_e (MeV)$=0.05\ I_{18}^{1/3}(I < 10^{18}$ W cm$^{-2})$ [33], where E is the electron energy, T_e is the electron temperature, I_{18} is the laser intensity in units of 10^{18} W/cm^2, and $\lambda_{\mu m}$ is the laser wavelength in micrometers. The energy loss of the fast electrons is described by a continuous slowing-down approximation, appropriate for cold, solid-density copper. Relativistic corrections to the copper K-shell ionization cross section are included [34].

For intensities $I > 10^{17}$ W/cm^2, the $K\alpha$ production efficiency is predicted to decrease with increasing laser intensity if refluxing is neglected. This is shown in Fig. 1(a) by the dashed curve for a laser-to-electron-energy-conversion efficiency $\eta_{L\to e}=40\%$. The fast electrons become less collisional as their energy increases, and progressively fewer K-shell vacancies are produced before the electrons escape the target. This is because the target is thinner than the electron range. On the other hand, if electrons reflux and lose the bulk of their energy in the target, regardless of their range, the predicted $K\alpha$ efficiency is a weakly increasing function of laser intensity for $I > 10^{18}$ W/cm^2. This is shown in Fig. 1(a) for various $\eta_{L\to e}$ (solid lines) and is a result of the energy dependence of the fast-electron range and the K-shell ionization cross section. Importantly, measurements of $K\alpha$ production efficiencies in this regime are insensitive to the fast-electron temperature and energy spectrum. Refluxing from sheath fields is considered to be responsible for this effect.

The fraction of fast electrons that are stopped inside the target has been estimated using a simple capacitance model based on that presented in Ref. [23]. The model considers the target potential drop due to fast electrons escaping a perfectly conducting thin disk in vacuum. Figure 1(b) shows the results of this model for the laser parameters and foil radii of interest to the current experiment. Refluxing efficiencies are predicted to be in the range $\eta_r > 95\%$. While modifications due to imperfect target isolation are not considered in the model, the analysis indicates that high refluxing efficiencies are to be expected. This is consistent with the results in Fig. 1(a).

Good agreement is found between the experimental data and the $K\alpha$ yield predictions from the refluxing model, assuming $\eta_{L\to e}=15\pm 7\%$ for laser intensities $I > 10^{18}$ W/cm^2.

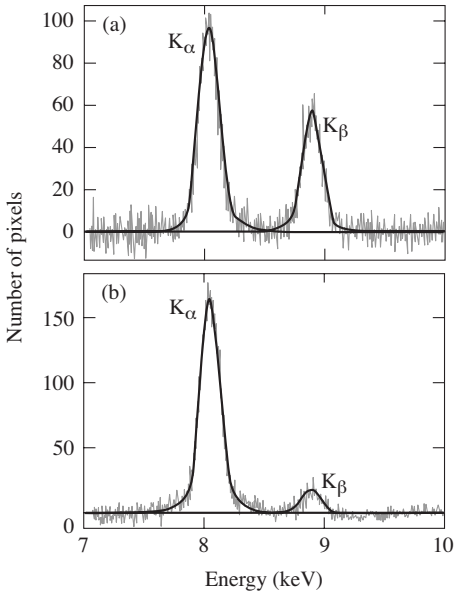

FIG. 2. K-shell spectra for (a) $(500\times500\times50)$-μm^3 and (b) $(20\times20\times3)$-μm^3 copper targets at laser intensity $I=2\times10^{19}$ W/cm^2.

If fast-electron refluxing is ignored, the discrepancy between the experimental data and the theoretical predictions would be greater than an order of magnitude in the predicted $K\alpha$ yield. $K\alpha$ efficiencies for laser intensities $I < 10^{17}$ W/cm^2 fall rapidly with decreasing intensity because the fast-electron temperatures fall below the energy threshold $E \sim 8$ to 9 keV required for the creation of K-shell vacancies. As a result, $K\alpha$ efficiencies in this intensity regime are very sensitive to the fast-electron temperature and the scaling law used to connect the fast-electron temperature to the laser intensity.

Fast-electron-energy transfer to the target bulk material, before significant decompression and hydrodynamic disassembly, makes it possible for the energy content of the fast electrons to be inferred. In our experiments, this is achieved by monitoring the change in the ratio of the number of emitted $K\beta$ and $K\alpha$ photons with respect to that found in the cold-material limit as the target volume is varied [22]. The target temperature and density determine the population of copper ions and alter the emission probability of the K-shell line radiation as a function of increasing energy density. In particular, depletion of the copper L and M shells at high plasma temperature, through collisional ionization with the thermal electron population, makes it possible for the fast-electron-energy content to be inferred and compared to that predicted in the cold limit.

Figure 2 shows two examples of copper K-shell spectra for (a) $(500\times500\times50)$-μm^3 and (b) $(20\times20\times3)$-μm^3 targets at laser intensities of 2×10^{19} W/cm^2. The K-shell spectra from each of these targets were filtered using 150 and 75-μm-thick copper foils, respectively. The copper $K\alpha$ (8.05 keV) and the copper $K\beta$ (8.91 keV) lines are well-resolved. A significant reduction in the absolute $K\beta$ yield is seen from the $(20\times20\times3)$-μm^3 target. This result is attributed to the higher-energy-density environment that has been created.

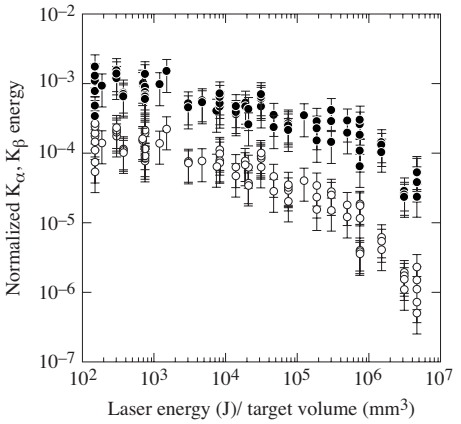

FIG. 3. Energy in $K\alpha$ (solid circles) and $K\beta$ (open circles) (normalized to the laser energy) as a function of laser energy (J)/target volume (mm^3) at a laser intensity $I=2\times10^{19}$ W/cm^2.

Figure 3 shows the systematic effect of decreasing the target volume on the *K*-shell fluorescence yields at a constant laser intensity of 2×10^{19} W/cm^2. The normalized $K\alpha$ and $K\beta$ yields are plotted as a function of laser energy divided by the target volume. Initially, both the $K\alpha$ and $K\beta$ yields remain approximately constant. The normalized $K\beta$ yield then begins to decrease at a greater rate compared to the $K\alpha$ yield. For the smallest mass targets, both the $K\alpha$ and $K\beta$ yields fall significantly below the cold-material value.

IV. ANALYSIS AND MODELING

Numerical modeling of the experiment was performed using the three-dimensional implicit-hybrid PIC code LSP [35]. It included the effects of fast-electron refluxing by self-consistently calculating the self-generated electromagnetic fields, the effect of spatial and temporal gradients on heating, and target expansion [23]. Laser coupling was modeled by promoting electrons from the cold bulk-electron background at a rate consistent with $\eta_{L\to e}$. A Thomas-Fermi equation-of-state model appropriate for copper plasma was used and, to ensure the $K\alpha$ and $K\beta$ emission probabilities were correctly weighed as a function of bulk electron temperature, the collisional-radiative code PRISMSPECT [36] was used to determine the target ion-population distribution. This is justified because the thermal background, not the MeV-scale fast-electron component of the distribution function, governs the charge-state dynamics in the plasma.

The experimental ratio, $K\beta/K\alpha$, is shown in Fig. 4(a) (normalized to the cold-material limit) as a function of target volume. For each target volume, the relative error in $K\beta/K\alpha$ is calculated from the standard deviation over a number of shots using the same laser pulse duration (1 ps) and laser intensity ($I=2\times10^{19}$ W/cm^2). The results in Fig. 4(a) are compared to LSP target-heating calculations to infer the fast-electron-energy content. Numerical results are given for $\eta_{L\to e}=10$ and 30% (dashed lines). The calculated variation of $K\beta/K\alpha$ with increasing bulk electron temperature is shown in Figs. 4(a) (right axis) and 4(b) (inset).

An important observation is the role of target area and thickness on the observed $K\beta/K\alpha$ ratio. It is shown in Fig. 4(b) that reducing the target thickness from 50 to 2 μm while maintaining a fixed target area of 500×500 μm^2 (dashed curve) does not heat the plasma beyond the cold-material limit. The effect of reducing the target area from 500×500 to 20×20 μm^2 at a constant 2-μm thickness (solid curve), however, produces dramatic bulk heating in the smallest-volume targets. Reducing the target thickness is necessary, but not sufficient, for creating the highest-energy-density conditions.

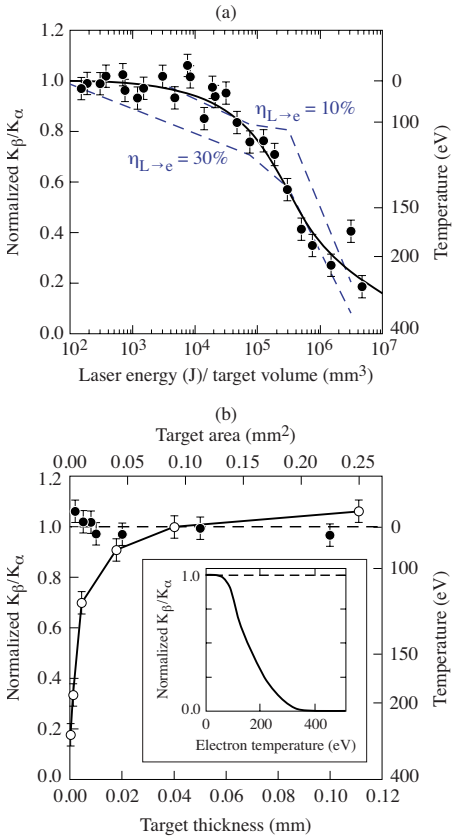

FIG. 4. (Color online) (a) Experimental $K\beta/K\alpha$ data [normalized to the cold-material value (left axis)] and inferred bulk-electron temperature (right axis) as a function of laser energy (J)/target volume (mm^3). Calculated $K\beta/K\alpha$ values are shown, assuming laser-to-electron-energy-conversion efficiencies $\eta_{L\to e}=10$ and 30% (dashed lines). (b) Experimental $K\beta/K\alpha$ data [normalized to the cold-material value (left axis)] and inferred bulk-electron temperature (right axis) as a function of foil area at constant thickness (2 μm) (lower axis, solid circles) and as a function of foil thickness at constant area (500×500 μm^2) (upper axis, open circles). (Inset) Calculated $K\beta/K\alpha$ variation with bulk-electron temperature (normalized to the cold-material value).

Figure 4 shows that for the highest energy density, target heating causes the $K\beta$ and $K\alpha$ emission probabilities to be significantly suppressed. The 5× reduction in $K\beta/K\alpha$ below the cold-material limit indicates electron temperatures greater than 200 eV according to the scaling shown in Fig. 4(b) (inset). The hot plasma will contribute negligibly to the total *K*-photon yields since the emission is naturally weighted toward higher densities. The total target mass is expected in all cases to be much greater than in the pre-plasma corona. For the smallest targets, however, the theo-

retical $K\beta/K\alpha$ predictions begin to converge for various $\eta_{L\to e}$, making an experimental comparison increasingly challenging. The reduction in $K\alpha$ signal for the smallest mass targets may indicate collisional ionization of the L shell, implying temperatures exceeding 200–300 eV.

Figure 4 shows broadly good agreement between the experimental and the calculated $K\beta/K\alpha$ values for $\eta_{L\to e}$ ~20% over a wide range of target volumes. Importantly, the inferred $\eta_{L\to e}$ represents a minimum value. (Under similar irradiation conditions, conversion efficiencies of laser energy into ions of a few percent have been reported [37–40], representing a small percentage-level energy correction due to ion acceleration effects.) The model comparisons presented here represent the minimum laser-to-electron-energy transfer that is required for refluxing to account for the observed bright K-photon emission.

V. SUMMARY

Collisional fast-electron energy transfer in the refluxing regime is an attractive route to future high-energy-density table-top plasma sources. Efficient bulk isochoric heating of solid-density material has been demonstrated to greater than 200 eV using a relativistic-intensity 5-J, 1-ps laser pulse. K-photon fluorescent probability suppression with increasing energy density, through strong modification of the cold $K\beta/K\alpha$ ratio, has been successfully used to probe the bulk plasma conditions created. The results and their interpretation are fully supported by three-dimensional, implicit-hybrid particle-in-cell simulations and collisional-radiative code modeling.

ACKNOWLEDGMENTS

This work was supported by the U.S. Department of Energy under Cooperative Agreements No. DE-FC52-08NA28302 (Office of Inertial Confinement Fusion) and No. DE-FC02-ER54789 (Fusion Science Center, Office of Inertial Fusion Energy Science), the University of Rochester, and the New York State Energy Research and Development Authority.

[1] S. C. Wilks, W. L. Kruer, M. Tabak, and A. B. Langdon, Phys. Rev. Lett. **69**, 1383 (1992).
[2] R. B. Stephens *et al.*, Phys. Rev. E **69**, 066414 (2004).
[3] K. B. Wharton, S. P. Hatchett, S. C. Wilks, M. H. Key, J. D. Moody, V. Yanovsky, A. A. Offenberger, B. A. Hammel, M. D. Perry, and C. Joshi, Phys. Rev. Lett. **81**, 822 (1998).
[4] K. Yasuike *et al.*, Rev. Sci. Instrum. **72**, 1236 (2001).
[5] F. N. Beg *et al.*, Phys. Plasmas **4**, 447 (1997).
[6] J. Fuchs *et al.*, Phys. Rev. Lett. **91**, 255002 (2003).
[7] E. Martinolli *et al.*, Phys. Rev. E **73**, 046402 (2006).
[8] A. Saemann, K. Eidmann, I. E. Golovkin, R. C. Mancini, E. Andersson, E. Forster, and K. Witte, Phys. Rev. Lett. **82**, 4843 (1999).
[9] S. P. Hatchett *et al.*, Phys. Plasmas **7**, 2076 (2000).
[10] B. A. Remington *et al.*, Science **284**, 1488 (1999).
[11] O. L. Landen *et al.*, Rev. Sci. Instrum. **72**, 627 (2001).
[12] H.-S. Park *et al.*, Rev. Sci. Instrum. **75**, 4048 (2004).
[13] H.-S. Park *et al.*, Phys. Plasmas **13**, 056309 (2006).
[14] H.-S. Park *et al.*, Phys. Plasmas **15**, 072705 (2008).
[15] M. Tabak *et al.*, Phys. Plasmas **1**, 1626 (1994).
[16] M. H. Key, Phys. Plasmas **14**, 055502 (2007).
[17] H. Alfvén, Phys. Rev. **55**, 425 (1939).
[18] A. R. Bell *et al.*, Plasma Phys. Controlled Fusion **39**, 653 (1997).
[19] K. Eidmann *et al.*, J. Quant. Spectrosc. Radiat. Transf. **81**, 133 (2003).
[20] R. A. Snavely *et al.*, Phys. Rev. Lett. **85**, 2945 (2000).
[21] R. G. Evans *et al.*, Appl. Phys. Lett. **86**, 191505 (2005).
[22] W. Theobald *et al.*, Phys. Plasmas **13**, 043102 (2006).
[23] J. Myatt *et al.*, Phys. Plasmas **14**, 056301 (2007).
[24] G. Gregori *et al.*, Contrib. Plasma Phys. **45**, 284 (2005).
[25] S. N. Chen *et al.*, Phys. Plasmas **14**, 102701 (2007).
[26] J. D. Hares, J. D. Kilkenny, M. H. Key, and J. G. Lunney, Phys. Rev. Lett. **42**, 1216 (1979).
[27] H. Chen *et al.*, Phys. Rev. Lett. **70**, 3431 (1993).
[28] S. D. Baton *et al.*, High Energy Density Phys. **3**, 358 (2007).
[29] V. Bagnoud *et al.*, Opt. Lett. **30**, 1843 (2005).
[30] V. Bagnoud *et al.*, Opt. Express **15**, 9 (2007).
[31] C. Stoeckl *et al.*, Rev. Sci. Instrum. **75**, 3705 (2004).
[32] H.-S. Park *et al.*, Phys. Plasmas **13**, 056309 (2006).
[33] P. Gibbon and E. Förster, Plasma Phys. Controlled Fusion **38**, 769 (1996).
[34] H. Kolbenstvedt, J. Appl. Phys. **38**, 4785 (1967).
[35] D. R. Welch *et al.*, Phys. Plasmas **13**, 063105 (2006).
[36] Prism Computational Sciences, Inc., Madison, WI 53711.
[37] A. J. Mackinnon, Y. Sentoku, P. K. Patel, D. W. Price, S. Hatchett, M. H. Key, C. Andersen, R. Snavely, and R. R. Freeman, Phys. Rev. Lett. **88**, 215006 (2002).
[38] L. Robson *et al.*, Nat. Phys. **3**, 58 (2007).
[39] P. K. Patel, A. J. Mackinnon, M. H. Key, T. E. Cowan, M. E. Foord, M. Allen, D. F. Price, H. Ruhl, P. T. Springer, and R. Stephens, Phys. Rev. Lett. **91**, 125004 (2003).
[40] J. Fuchs *et al.*, Nat. Phys. **2**, 48 (2006).